Spatial aerosol flow maldistribution: A design flaw confounding the proper calibration and data interpretation of stages "0" and "1" of the Andersen eight-stage nonviable cascade impactor

Daryl L. Roberts & Jolyon P. Mitchell

View supplementary material

Submit your article to this journal

View related articles

Accepted author version posted online: 23 Nov 2016.
Published online: 23 Nov 2016.

Article views: 17

View Crossmark data
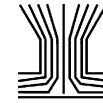
Spatial aerosol flow maldistribution: A design flaw confounding the proper calibration and data interpretation of stages "0" and "1" of the Andersen eight-stage nonviable cascade impactor

Daryl L. Roberts[a] and Jolyon P. Mitchell[b]

[a]MSP Corporation, Shoreview, Minnesota, USA; [b]Jolyon Mitchell Inhaler Consulting Services, Inc., London, Ontario, Canada

ABSTRACT

We introduced monodisperse calibrant particles into an eight-stage non-viable Andersen cascade impactor (ACI) operated at 28.3 L/min and separately quantified the particle mass captured under each of the four concentric rings of nozzles on stages 0 and 1, the entry and succeeding stages of this impactor. On both stages, we found that each ring of nozzles has a particle capture efficiency behavior that differs from the others, and the fraction of calibrant particles deposited under each of the individual rings of nozzles depended on the particle size. We believe this behavior derives primarily from a radial flow velocity non-uniformity associated with recirculation zones introduced by the 110° expansion angle of the inlet cone. Because of these recirculation zones, the inertia of particles larger than about 5 μm aerodynamic diameter will cause their point-wise local concentration to differ from the concentration at the inlet entry. This concentration maldistribution continues to stage 1 primarily because of the annular collection plate at stage 0. The influence of the inlet cone aerodynamics on the performance of both stages means that the size of particles deposited on these plates will be uncertain unless the aerosol transport entering the impactor associated with calibration using monodisperse particles exactly simulates the in-use aerosol flow conditions. The degree of realism necessary in the calibration method has heretofore not been discussed in published calibrations of the ACI, introducing uncertainty in the size interpretation of the particle mass collected on stages 0 and 1 in practical applications of this impactor.

Introduction

Multi-stage cascade impactors are widely used for characterizing the size properties of aerosol particles emitted from inhalable drug devices such as pressurized metered-dose inhalers (pMDIs) or dry-powder inhalers (DPIs) because they directly measure aerodynamic diameter, which is the most relevant parameter to describe particle transport within the respiratory tract (Mitchell and Nagel 2003). Impactors do not represent a model of the human respiratory tract, but the inertial size-separation of particles that takes place in an impactor is the same process governing a major portion of the deposition of inhaled particles (Dunbar and Mitchell 2005). Importantly, the cascade impaction method allows the user to determine the chemical identity of the particles collected on each stage, giving a reasonable understanding of whether the active pharmaceutical ingredient (API(s)) in the inhaler being evaluated is/are indeed present in particles that are likely to penetrate into the lung (Christopher et al. 2003).

Historically, the Andersen eight-stage non-viable impactor (ACI; Andersen 1958), with the uppermost two stages, designated "0" and "1" in the configuration operated at a nominal flow rate of 28.3 L/min, and modified by McFarland et al. (1977) to reduce inter-stage losses, subsequently became one of the most widely used cascade impactors for testing inhalable aerosols (Mitchell and Nagel 2003; Byron et al. 2004). However, it should be noted that many new drug products are now being tested with the Next Generation Impactor (NGI), developed purposely for size-fractionating aerosols from inhalers (Byron et al. 2004; Son et al. 2011). The ACI has been calibrated at 28.3 L/min with monodisperse aerosols by several authors, in particular by Mitchell et al. (1987) and Vaughan (1989), and is used at this flow rate for the evaluation of pMDIs. The same stage configuration may also be operated at 60 L/min for the evaluation of DPIs, with appropriate adjustments to the stage cut-off sizes (Mitchell and Nagel 2003). Although some differences exist between reported calibrations of this type,

there is a preponderance of data sufficient to impart a reasonable degree of confidence in the stage cut-point sizes (D_{50} values) reported in the compendial literature (United States Pharmacopeia 2016; European Pharmacopoeia 2016).

Previous investigations related to the behavior of the ACI in DPI testing indicated that the flow velocity profile entering the nozzle plates of the uppermost stages (stages "0" and "1") is nonuniform (Mohammed et al. 2012). It is pertinent to the present investigation to be aware that the circular collection plates associated with these stages are annular, rather than solid, as is the case for collection plates for stages "2" to "7" of this impactor. This finding of flow nonuniformity subsequently led us to investigate experimentally (Roberts and Mitchell 2014) why the first two stages of this impactor, when operated at 28.3 L/min, exhibit an obvious visual flow maldistribution among the four rings of nozzles (mapped in Figure 1). Examples of this behavior are shown in Figure S1 (see the online supplementary information [SI]). In Figures S1a and S1c (stage "0" with 11-μm particles and stage "1" 8-μm particles respectively), the maldistribution is quite subtle because the particles sampled are much larger than the cut point size of the stage, and therefore the deposits appear roughly visually equivalent at each ring. However, in Figures S1b and S1d (stage "0" with 8-μm particles and stage "1" with 5-μm particles, respectively), the inequality of the ring deposits becomes quite visually evident since the particles are smaller than the stage cut point size (as given in the USP 2016), which we will show is an "average," of a sort, of the individual ring cut-point sizes.

Similarly maldistributed deposition patterns of polydisperse phosphor particles were observed by Vaughan (1989) when viewed in ultra-violet light as part of his calibration of an ACI (Figure S2 in the SI). However, images of his deposits were not published in the original article, as the focus of that work, apart from determining the stage collection efficiency curves, was on estimating total losses due to internal wall deposition. Importantly, however, in the context of our decision to confine the scope of the present investigation to just stages "0" and "1", Vaughan observed that the radial deposits for stages 2 and below appeared to be more uniform. There was some evidence of "streaking" in the outward direction, most likely caused by cross-flow moving toward the periphery of these solid surfaced (not annular) disk-shaped collection plates.

We note here that the observed streaks and maldistribution of deposits take place even though the cross-flow parameters for these two stages, 0.82 and 0.62, respectively, are well below the critical value of 1.2 described by Fang et al. (1991). The cross-flow parameter is meant to assess whether the individual nozzles are operating independently of each other. Our observation may indicate that this parameter by itself may therefore not be as

reliable of a predictor of nozzle independence as has been thought, particularly in the presence of flow maldistribution, but further investigation of this matter is outside the scope of the present investigation.

Given these observations, we devised a method to quantify the mass of monodisperse calibrant aerosol captured under each of the four rings of nozzles on stages 0 and 1 of the ACI, the results of which are reported herein. During this development, it became evident that maldistribution in the magnitude of the flow velocity profile approaching each nozzle plate of stages "0" and "1" alone could not explain the results from the present study nor our initial study (Roberts and Mitchell 2014). A goal of the present study, therefore, is to develop a deeper mechanistic understanding of the underlying causes for the maldistributed deposits.

Experimental methods

We generated monodisperse liquid particles of uranine-tagged oleic acid with a Model 1520 Flow-Focusing Monodisperse Aerosol Generator (FMAG; MSP Corporation, Shoreview, MN, USA; Duan et al. 2016). This source of calibrant aerosols is highly stable compared to the traditional vibrating-orifice approach to making monodisperse aerosols described by Berglund and Liu (1973) and commercialized currently as the Model 3450 VOAG (TSI Incorporated, Shoreview, MN, USA). The key to the stability of the FMAG is that the nozzle creating the jet of monodisperse droplets is large, approximately 100 μm in diameter, and therefore less susceptible to clogging. The FMAG also provides its own charge equilibration via bi-polar corona discharge, eliminating the conventional krypton-85 radioactive ionization chamber that is essential with the VOAG method. We passed the aerosol from the FMAG through a custom-built single-stage impactor designed to remove doublets (Siegford et al. 1994), and we confirmed the particle size and monodispersity with a Model 3321 Aerodynamic Particle Sizer (APS; TSI Inc.).

We selected a complete and unused ACI (Copley Scientific Ltd., Nottingham, UK), whose nozzles had been inspected optically at the time of manufacture. For the purposes of this study, all 96 nozzles on stages "0" and "1" were considered identical in size, 2.55 mm and 1.89 mm in diameter, respectively. Before introducing calibrant aerosol particles, we set the air flow rate at the inlet entry to 28.3 $\pm$ 0.4 L/min using house vacuum and a control valve. We checked the flow rate through the apparatus before each measurement by means of a Model 4043 mass flow meter (TSI Inc.) located at the inlet.

We provided approximately 15 L/min of dilution air to the FMAG, and this air flow evaporated the oleic acid diluent (methanol) and carried the monodisperse and charge-equilibrated particles through the doublet
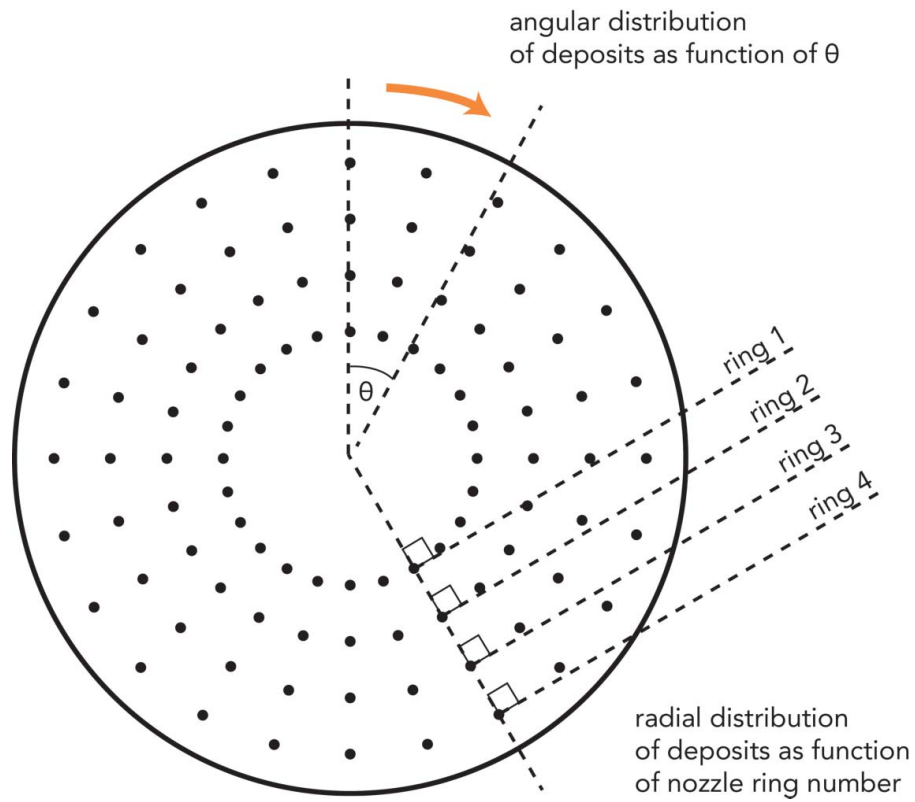
Figure 1. Plan view of Stage 0 or 1 of the ACI defining angular and radial nozzle arrangement.
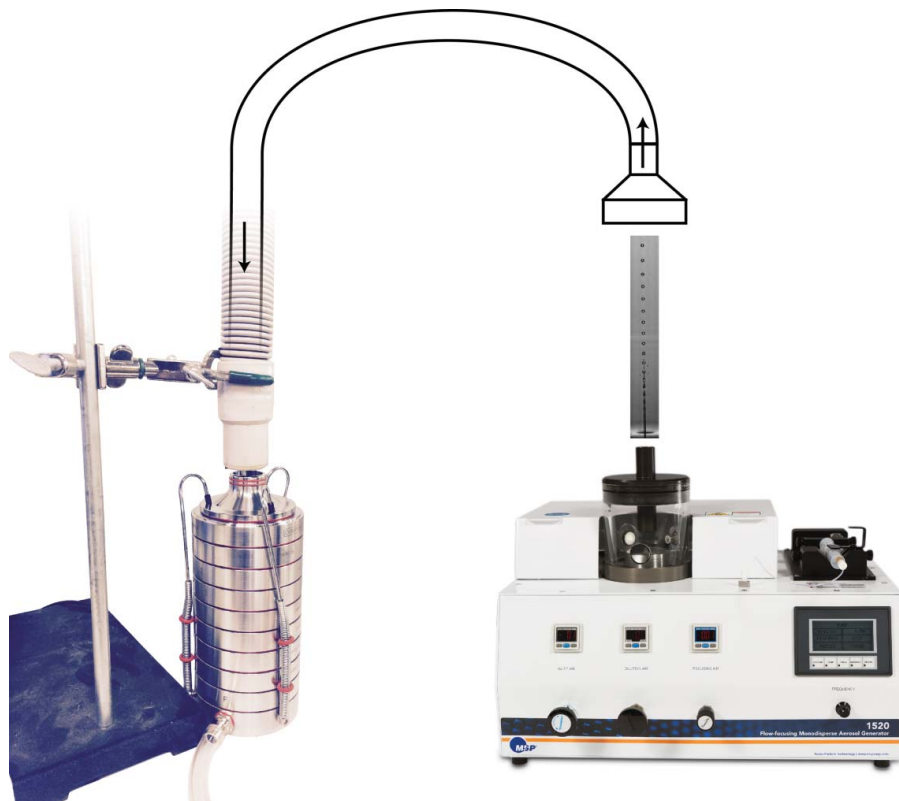
Figure 2. Generation of calibrant particles and introduction to impactor inlet.

eliminator to the inlet of the impactor (Figure 2). We located the aerosol tube exit above the impactor inlet, introducing the 15 L/min of aerosol-laden air along with the balance of the 28.3 L/min air flow from room air. The inside diameter of the aerosol delivery tube was 31.75 mm, and this delivery tube was centered over the cone inlet, which has an inside diameter of 25.4 mm.

The compendial D_{50} values of stages 0 and 1 are 9.0 μm and 5.8 μm, respectively, at a nominal flow rate of 28.3 L/min (United States Pharmacopeia 2016; European Pharmacopoeia 2016). Consequently, we generated particles that had nominal count median sizes (as measured by the APS) between 5 and 11 μm aerodynamic diameter, and determined the particle capture efficiency curves for stages "0" and "1" separately, according to standard uranine tracer-based methods (Marple et al. 2003b). We tested stage "0" with particles having nominal sizes of 8, 9, 10, and 11 μm aerodynamic diameter, and we correspondingly evaluated stage "1" with particles having nominal sizes of 5, 9, 10, and 11 μm aerodynamic diameter. In all cases, the ACI was assembled in its entirety, as shown in Figure 2.

In the first phase of our investigation, we washed the *entire* stage plate to measure the particle capture efficiency curve of the stage as a single entity, as would be done in normal calibration and use of the impactor. This work yielded the "mass-average" capture efficiency curve, so-named to distinguish from the capture efficiency of the individual rings of nozzles. This method is typical of techniques for calibrating impactors as described by Mitchell et al. (1987) and Vaughan (1989) for the ACI and by Marple et al. (2003b) for the NGI. The results closely mirrored our previous results (Roberts and Mitchell 2014), in agreement with the D_{50} values reported in the USP and the EP for stages 0 and 1 of the ACI, and therefore giving confidence that our experimental methodology was correct.

Our main goal, however, was to determine the capture efficiency *separately* for each of the four rings of nozzles on these stages. So, for the bulk of our study, we used separate Q-tips wetted with isopropanol to recover manually the calibrant particle deposits on the collection plate of stage "0" and of stage "1", where the ring numbering sequence is defined in Figure 1. We accomplished the quantification of the deposit mass associated with each ring by first wiping the deposits below the outermost ring 4 with the isopropanol-soaked Q-tip(s), secondly wiping the deposits beneath ring 3, then wiping the deposits under ring 2, and finally, wiping those beneath the innermost ring 1. Often, more than one Q-tip was needed to remove the deposits entirely from a given ring. We repeated the process for stage 1, recovering the deposited particle mass from beneath the

separate nozzle rings of stage "1". Subsequently, the recovered particle mass from each of the eight samples was dissolved in a known volume of isopropanol, and the concentration of uranine was determined fluorometrically. We expressed the individual values of uranine mass in fractional terms based on the total captured uranine mass deposited under all nozzles of the stage under evaluation. We observed that a trace amount of residual "smeared" deposit always persisted on the surface of the collection plate associated with each stage, following recovery of the particles located beneath the nozzles. Despite this observation, the experimental repeatability we achieved by the chosen procedure was sufficient to deduce the behavior of interest.

Results

In our initial study (Roberts and Mitchell 2014), we noted that our stage efficiency curves for ACI stages "0" and "1", determined at a flow rate of 28.3 L/min (Figure 3), agreed

(a)

(b)
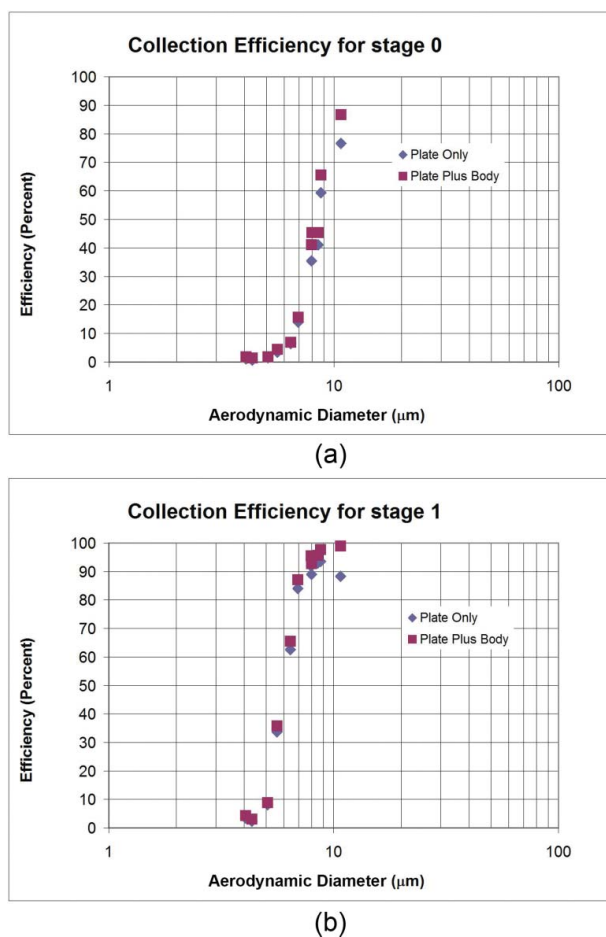
Figure 3. Measured particle capture efficiency curves for (a) Stages "0" and (b) "1" of the Andersen impactor operated at 28.3 L/min (Roberts and Mitchell 2014); the D_{50} values are 9.0 and 5.8 μm, respectively, in agreement with the generally accepted values (USP, Ph. Eur.).

rather well with the corresponding data reported by Vaughan for these stages (see Figure 6 and Table 3 of Vaughan [1989]). Our data show that internal wall losses associated with either stage (plate + body) were small, such that the curve we obtained for each stage, when losses were included in the assessment, was superimposable on the corresponding collection efficiency curve derived if only the mass of calibrant recovered from the collection plate had been considered.

In the current investigation, when quantifying the mass on the individual rings of deposits, we found that the deposits were not only highly unequal in mass recovered from one ring to another, but the mass fraction deposited beneath each nozzle ring changed with the size of the calibrant particle (Table 1). Typical deposits on the collection plates before the wiping of the deposits with isopropanol-soaked Q-tips are shown in Figure S3 (see the SI).

The striking nonuniformity in deposition is well illustrated in the mass fraction values for stage "0" obtained with 9-μm diameter particles (close to the nominal cut-point size for this stage); these values varied from 6.8% at ring 3 to 68.0% at ring 1, a ten-fold difference. The change in this maldistribution with particle size is also evident; for example in ring 1 of stage "0," the deposited mass fraction changed from 53.5% to 77.7% for particles having nominal sizes of 8.0 and 10.0 μm aerodynamic diameter respectively. A similar trend was evident for the innermost ring of stage "1", where the deposited mass fraction varied from between 40 and 42% for the 5.0- and 9.0-μm diameter particles to 64.8% for the 11.0-μm diameter particles. Corresponding decreases in mass as calibrant particle size increased were most evident for outer rings 3 and 4 of stage "0", and also with ring "4" of stage "1." The mass fraction of calibrant recovered from intermediate ring 2 of either stage was largely unaffected by changes to calibrant particle size, with the exception of

Table 1. Capture of various sizes of monodisperse microsphere calibration aerosols under each concentric ring for collection plates relating to stages "0" and "1" of an ACI operated at 28.3 L/min.

Aerodynamic diameter of calibrant particle (μm)	Stage	Mass of calibrant collected under the indicated ring of nozzles as fraction of total mass on all rings (%)			
		Ring 1	Ring 2	Ring 3	Ring 4
8.0	0	53.5	14.1	13.1	19.2
9.0		68.0	12.9	6.8	12.4
10.0		77.7	11.6	3.6	7.0
11.0		74.4	16.4	3.9	5.4
5.0	1	41.8	10.2	15.5	32.4
9.0		40.1	24.3	16.6	18.9
10.0		48.6	25.4	15.9	10.1
11.0		64.8	20.4	8.1	6.7
Ideal Behavior Irrespective of Calibrant Size					**25.0**

Table 2. Repeatability of deposit recovery from ACI stages "0" and "1"; the mean and standard deviation for deposit mass fraction (%) are identified in relation to nozzle ring number.

Stage and particle size (μm)	Recovered particle mass fraction (%) of total mass of calibrant deposited on the stage (Mean $\pm$ S.D.)			
	Ring 1	Ring 2	Ring 3	Ring 4
0, 9.0	68.0 $\pm$ 6.1	12.9 $\pm$ 1.9	6.8 $\pm$ 2.3	12.4 $\pm$ 3.4
1, 9.0	40.1 $\pm$ 5.5	24.3 $\pm$ 2.1	16.6 $\pm$ 2.4	18.9 $\pm$ 4.7
1, 5.0	41.8 $\pm$ 5.0	10.2 $\pm$ 1.2	15.5 $\pm$ 2.5	32.4 $\pm$ 2.1

a low value close to 10% obtained for stage "1" with the smallest (5.0 μm) particles. Taken as an ensemble, these findings provide evidence of a skewing of the deposited calibrant particles from the innermost ring to the outer rings for both stages, as the particle size decreased.

An even distribution of air flow and an absence of particle concentration maldistribution within that air flow upstream of each nozzle plate, as assumed in impactor theory (Marple 1970; Marple and Liu 1974) would result in precisely 25% of the deposited mass on each ring, regardless of the size of the calibrant particles. This outcome is denoted in Table 1 as "ideal behavior." The observed behavior is substantially different than this "ideal" behavior.

We also tested the experimental repeatability by performing in triplicate the deposition and recovery of 9.0 μm aerodynamic diameter particles from stage "0", of the same sized particles from stage "1", and also of 5.0 μm aerodynamic diameter particles from stage "1" (Table 2). Standard deviation values were always less than 25% of the mean, and many were close to 10%, indicating that the macroscopic behavior we observed, for example in Figure S3, was repeatable.

Discussion

Qualitative interpretation of the experimental data

It is worthwhile considering how the visual impression of the maldistributed deposits of monodisperse calibrant particles compares to the quantitative data. Given that the nominal D_{50} value of stage "0" is 9.0 μm aerodynamic diameter, it is reasonable to expect to see deposits of such particles both on stage "0" and on stage "1." We did in fact observe such behavior. The deposits appear focused to the innermost ring (ring 1) for stage "0" (Figure S3a), but they are more evenly distributed on the collection plate for stage "1" (Figure S3c). This visual impression is consistent with the 9-μm mass deposition data for stage "0" distributed by ring number, that varied from 6.8% to 68.0% for this stage, compared with the range from 16.6% to 40.1% for stage "1" (Table 1). We believe that the more uniform-looking deposits between

the nozzle rings for stage "1" are to be anticipated because the D_{50} value of this stage (5.8 μm) is much smaller than the incoming particle size. Under such circumstances, every ring would be expected to be active at collecting the incoming particles from stage "0". And, looking at Figure S3 and at the data in Table 1 closely, it is evident that the eye is not readily able to distinguish quite significant differences in the deposited mass fraction. This observation may help explain why the maldistribution in deposit mass recovered quantitatively from ring to ring has gone unreported, given the polydispersity of most aerosols evaluated in normal use of the ACI.

The behavior of the largest 11-μm aerodynamic diameter particles passing through both stages visually indicates that the flow maldistribution persisted to stage "1" (compare Figures S3b with S3d), in accordance with the data in Table 1. It can be argued that the observed flow maldistribution is less for stage "1", but this point is not critical to our discussion. We believe it is likely that the potential for persistence in radial flow non-uniformity to stage "1" arises as the result of the circular hole in the central region of the collection plates of both stages (they each have an annular shape).

We believe the primary physical explanation underlying our observations is HOW the aerosol enters the cone of the ACI. The importance of this cone lies in the behavior of the laminar jet formed when the air expands into the internal space of the cone before entering the nozzles of stage "0". We consider first the situation where the incoming air stream is uniformly distributed across the entrance of the cone. The flow Reynolds number at the entrance of the cone is 1670 at 28.3 L/min, suggesting laminar flow exists at that location. It is well understood (Blevins 1984) that a smooth expansion of a laminar jet takes places if the expansion angle is smaller than 15° in a regular expanding cone-shaped geometry, as illustrated in Figure 4a. As the angle increases beyond 20°, flow separation at the wall begins (Figure 4b), leading to the formation of recirculation zones when the expansion angle exceeds 40° (Figures 4c and d). However, the interior angle of the ACI cone, at 110°, is much greater than this critical angle for the onset of non-ideal behavior, ensuring that both a focused jet flow and flow recirculation zones are formed (Figure 4e). Hence, individual particle trajectories in flight are prematurely separated on the basis of their aerodynamic size because of their differing inertia, as the incoming and descending air flow at the base of the recirculation turns back toward the entrance to the inlet to the ACI. This nonideal process results in a simultaneous focusing of large particles toward the central axis of the pathway from the inlet entry to the nozzles of stage "0", as depicted in Figure 5. Likewise, smaller particles are selectively moved toward the periphery of this pathway, before they pass through the nozzles themselves. Under such circumstances, the outermost nozzle ring 4 will receive preferentially the smaller particles more than the larger ones, as we observed in the deposition data presented in Table 1. Conversely, larger particles will be more efficiently collected than smaller sized particles at the innermost ring 1, a finding also observed in the same data set.

A similar mechanism appears to be operating upstream of the nozzle plate of stage 1, although the geometry of the cavity occupied by the air flow between stages "0" and "1" is more complex (e.g., Figures 12 and 13 of Flynn et al. 2015). On this occasion, space formed by the central large hole in the collection plate of stage "0" allows short-circuiting of the air flow from the collection plate of stage "0" to the nozzles of stage "1", another key issue that we believe affects the capability of the upper stages of the ACI to function as intended. Furthermore, there is the suggestion of a greater tendency for deposition of the smaller particles to be augmented on the outermost ring 4 of stage "1", since a portion of the total air flow also passes around the periphery of the collection plate of stage "0" on its way to the nozzle plate of the following stage. Again, this explanation is consistent with the data presented in Table 1. Therefore we believe that pre-classification is indeed occurring in the space between the collection surface of stage "0" and the nozzle plate of the succeeding stage.

The interpretation of our findings reported in Table 1 is consistent with several related studies. For example, the apparent short circuiting of flow associated with stages fitted with annular collection plates was attributed by Mohammed et al. (2012) to the anomalously short interval between the start of sampling and particle transfer through the ACI in the testing of DPIs. Their conclusion was based on consideration of the time that should have been taken based on the magnitude of the internal dead space of this apparatus. Versteeg et al. (2015) also confirmed the presence of flow short-circuiting at an inlet flow rate of 60 L/min, typical of DPI testing.

Our findings are also consistent with the results from numerical simulations of the flow through the ACI that have identified radial flow velocity non-uniformity with this impactor, in simulations undertaken at both 28.3 L/min and 60 L/min (Flynn et al. 2015; Dechraksa et al. 2014). Importantly, such non-ideal behavior was identified when the conventional inlet cone, rather than the pre-separator, was present, as in our study. Here, the air velocity streamline analyses in both studies clearly predicted recirculation zones in the space immediately above stage "0". Dechraksa et al. claimed, as we have done in the foregoing analysis of data from our study, that this flow pattern induced recirculation that affected
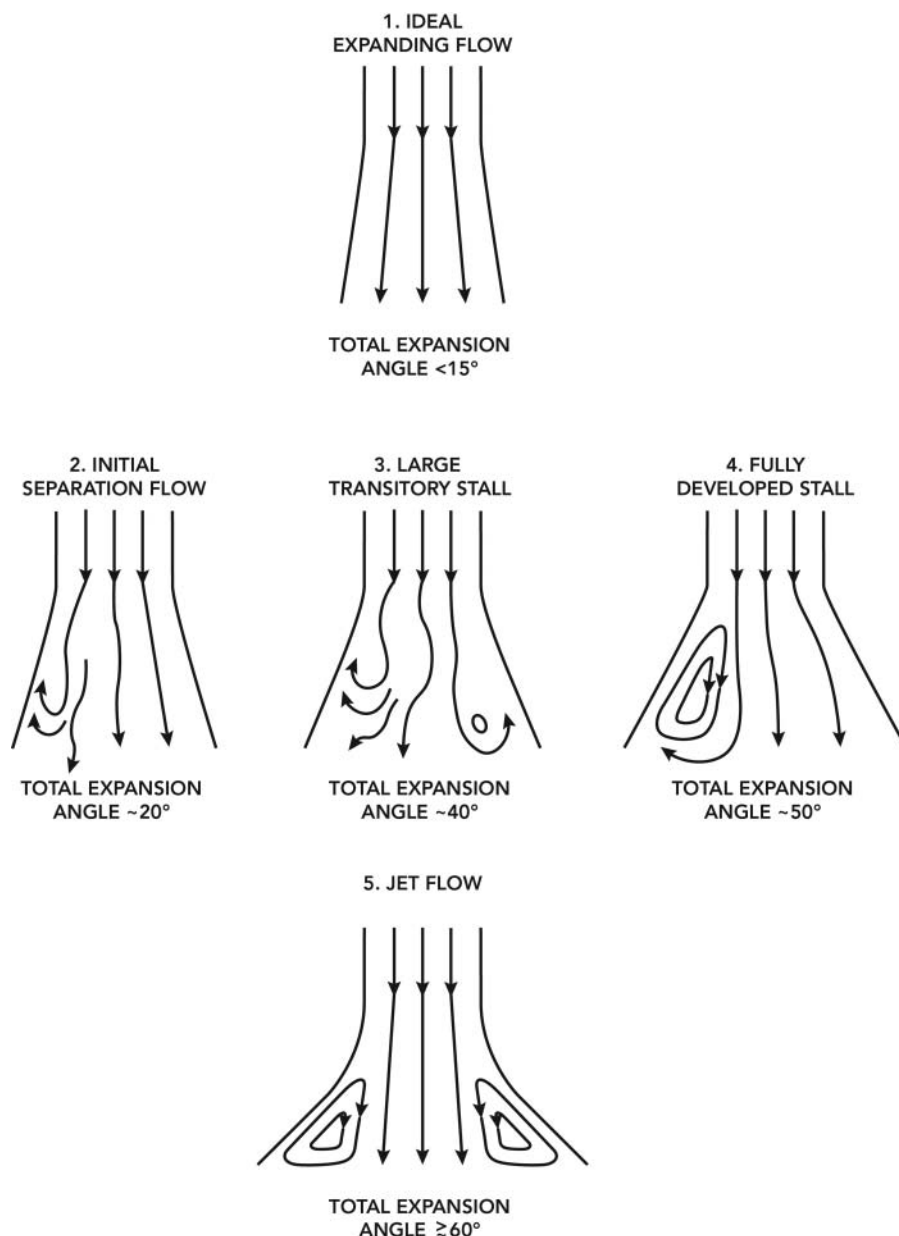
Figure 4. Air patterns in laminar jet expansion (simplified from Table 7–6 of Blevins, 1984).

the motion of incoming aerosol particles in a way that was dependent on their size. As a result, the normal size-fractionation process taking place between the exit of the nozzle plate and collection plate associated with this stage was perturbed. Furthermore, their images of the shear stress distribution associated with the collection plate under stage "0", derived by modeling the inlet cone configuration at a flow rate of 28.3 L/min are remarkably similar to the deposit distribution profiles we have presented in Figures S1 and S3 for this stage.

Non-uniformity in the radial flow velocity profile immediately above the nozzle plate guarantees that the D_{50} size assigned to each ring location will differ from each other, and also from the mass-average stage

efficiency curve determined by conventional calibration methods, such as shown in Figure 3. It is evident from inspection of the visual data of Figure S3, taken with the associated calibrant mass fraction depositions reported in Table 1, that rings 1 and 4 have the smallest and second smallest D_{50} values respectively. So, it follows that rings 2 and 3 therefore likely have D_{50} sizes larger than the mass-average D_{50} for that stage. At first sight, it would be ideal for either of the stages of interest, if we could deduce the complete particle capture efficiency curve for each ring. However, we cannot devise a consistent model of the particle size fractionation behavior for each ring *unless* we also postulate that the point-wise mass concentration of each of the monodisperse
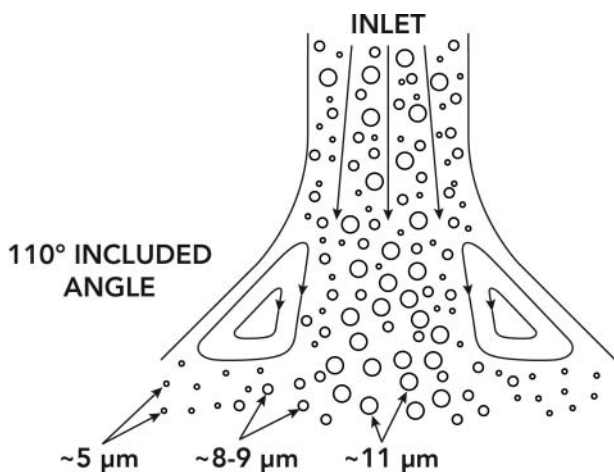
Figure 5. Schematic diagram of effect of particle inertia on localized mass concentration and size distribution of particles in the cone expansion inlet of the ACI; the larger inertia of the largest particles concentrates them in the central region above the entry to the nozzles, whereas the finest particles move with the circulating flow toward the periphery.

calibrant aerosols located immediately above the entire surface of the nozzle plate varied from the mass concentration at the entry to the inlet. This additional hypothesis is certainly plausible for particles possessing significant inertia, such as those larger than about 5 μm aerodynamic diameter, that are most likely to be size-fractionated by these stages. Such behavior would be in keeping with the well-understood observation that particles with appreciable inertia move preferentially, even under laminar flow conditions, toward the periphery of the passageway in a 90° elbow placed at the distal end of a tube through which the aerosol is flowing (Pui et al. 1987). If we accept the hypothesis for the presence of a skewed particle mass concentration profile above the entry to the nozzle plate of stage "0", as a result of inertia, we are led by both the visual and quantitative data to conclude that the mass concentration of the monodisperse aerosol entering the nozzles of ring 1 of this stage exceeds that of the inlet aerosol (forward inertia concentrates the particles). Furthermore, this process may in consequence deplete the mass concentration of the same aerosol entering the nozzles of ring 2 (and perhaps ring 3), ultimately relocating the remaining airborne particles out to ring 4 at the periphery of the collection plate.

We have mentioned this hypothesis regarding radial airborne particle concentration maldistribution, because it is distinct from merely identifying radial non-uniformity in the flow-velocity profile above the nozzle plates of the stages of interest. Indeed, the mass concentration of aerosol is well below that required to influence the flow; that is, we are nowhere near two-phase flow conditions (Govier and Aziz 1972). Inertial phenomenon are

indeed capable of inducing local non-uniformity in airborne particle concentration (for example, as in virtual impactors; Marple and Chien 1980). The data in Table 1 are difficult to derive without an appeal to such a cause of the observed maldistribution associated with the collected particles. It is essential to be aware that our data indicate that both the airborne size fractionation process and ensuing mass concentration maldistribution occur in the gas phase before the air flows through the nozzles of *both* stages "0" and "1" of the ACI. So the size distribution and mass concentration of particles entering each ring of nozzles will differ from the aerosol concentration *and* size distribution at the inlet entry plane, and will also change from ring to ring. And our work with monodisperse particles shows that the D_{50} values associated with each nozzle ring are different for these affected stages, and are not equal to the commonly determined mass average values. It therefore follows that the mass of an aerosol having unknown aerodynamic particle size properties captured on the collection plate of either stage will depend heavily on *how* the aerosol enters the cone.

For example, the flow fields sketched in Figures 4 and 5 are axisymmetric—but the flow field entering the cone after the discharge of aerosol from a pMDI canister and after passing through the USP/Ph.Eur. induction port (United States Pharmacopeia 2016; European Pharmacopoeia 2016), or through more recently developed abbreviated or more complex methods simulating human anatomy, is certainly not axisymmetric (Zhou et al. 2011). Rather the air flow stream skews to one side of the induction port when it makes its 90-degree turn, much like air flow in a 90-degree elbow (Pui et al. 1987). The degree to which the air flow skews to one side versus the other affects the radial maldistribution of particles and air flow velocities approaching the rings of nozzles on stage 0. The overall stage efficiency curve for stage 0 is therefore not known from a calibration with monodisperse particles introduced uniformly into the cone of the impactor, as is the case in common methods of impactor calibration, such as those reported in the literature for this impactor (Mitchell et al. 1987; Vaughan 1989).

The overall meaning of our experimental data, then, is that the stage efficiency curves for stages 0 and 1 are at best obscured and quantitatively uncertain, because of the combination of flow maldistribution in the cone and the different D_{50} values of the individual rings.

The quantitative conundrum

It is a simple matter to show that non-uniformity in the radial flow above the nozzle plate of a given cascade impactor stage introduces unknowns into the factors that determine the size of particles captured on a given

stage, whether these aspects affect only the D_{50} of each nozzle or ring of nozzles, or whether they also affect the local mass concentration and size distribution of the aerosol entering each nozzle or ring of nozzles.

Each data point of the conventional calibration of a cascade impactor with monodisperse aerosols yields the fraction of particles of a given size that are captured on the stage, which we give the symbol $F(d_{ae})$, noting that this fraction depends on the aerodynamic particle diameter. As a general rule, it is not necessary to postulate that all nozzles on a give stage are exactly the same size, and in common practice, the fraction $F(d_{ae})$ is fundamentally a sum of the flow weighted average efficiency of each nozzle (or ring of nozzles), as in Equation (1) (see Roberts 2009; Equation (2)):

$$F(d_{ae}) = \frac{\sum_{i=1}^{N} A_i U_i E_i(d_{ae})}{\sum_{i=1}^{N} A_i U_i} \quad [1]$$

Here A_i is the area of each individual nozzle, $E_i(d_{ae})$ is the efficiency with which a particle of aerodynamic diameter d_{ae} is captured under an individual nozzle, and U_i is the average velocity of air passing through an individual nozzle. This equation allows the individual nozzles to have individual particle capture efficiency curves, $E_i(d_{ae})$, that differ from the mass-average particle capture efficiency curve of the stage. From this formulation, we can deduce how the D_{50} of the stage is related to the diameters of each nozzle in the array in a multi-nozzle stage (Roberts 2009), such as is encountered with the uppermost two of the ACI that are of interest in the context of this present investigation.

However, implicit in this analysis is the hypothesis that the velocity of air through each nozzle is the same – that is, there is no significant radial flow velocity non-uniformity. This hypothesis is reasonable so long as the pressure drop across each nozzle is large compared to the pressure loss in distributing the aerosol into the plenum above the nozzles at each stage. The values of pressure drop of the nozzles for both stages "0" and "1" of the ACI are 4 Pa and 15 Pa respectively, sampling at a flow rate of 60 L/min, and are therefore quite small. If the flow rate is reduced to 28.3 L/min, we can expect the nozzle pressure drop to be reduced to about 1 Pa and 4 Pa for stage "0" and "1" respectively, in accordance with Roberts et al. (2006). These extremely small nozzle pressure drop values increase the ability of other fluid mechanical forces, such as collision of the incoming air jet with the plane of the stage 0 nozzles, to dominate the flow pattern leading up to the nozzles. Consequently, radial flow non-uniformity is both a logical and real process to be expected for both stages of interest in our

evaluation of the size-fractionating ability of the upper components of the ACI. Our experimental observations confirm that this non-ideal behavior is present. We can therefore no longer assume that the volumetric flow rate through each nozzle or ring of nozzles for either stage "0" or "1" is the same, *even if* we allow the hypothesis that each nozzle in the array has an identical diameter. Hence, in the presence of such non-uniformity in the flow velocity profile and, for simplicity, letting each nozzle be identical, Equation (1) can be written:

$$F(d_{ae}) = \frac{\sum_{i=1}^{N} U_i E_i(d_{ae}, U_i)}{\sum_{i=1}^{N} U_i} \quad [2]$$

Here, we have specifically noted that the particle capture efficiency for each nozzle or ring of nozzles depends on the particle size and also the velocity of air through the nozzle. This dependence on inlet air velocity, U_i, is always the case, but is not worth noting when the velocity of the flow through all the nozzles is identical.

In typical data analyses for cascade impactors, all particles approaching a given size-fractionating the stage are regarded as being larger than the D_{50} value of the stage, and smaller than the D_{50} value of the previous stage (Mitchell and Nagel 2003). The difference between this approximate approach to data analysis and more rigorous data inversion methods has been shown to be negligible in the context of testing inhalers (Roberts and Mitchell 2013). So, the common data interpretation of the size-fractionating function of stage "0" of the ACI is that all the particles assigned to this stage are larger than the mass-average D_{50} determined by the calibration with monodisperse particles. However, when the U_i values differ across the nozzle array, as we believe to be the case in actuality, the particles that are ACTUALLY captured with 50% efficiency are those that (implicitly) satisfy Equation (3):

$$0.5 = \frac{\sum_{i=1}^{N} U_i E_i(d_{ae}, U_i)}{\sum_{i=1}^{N} U_i} \quad [3]$$

The problem is that this equation cannot be solved analytically unless the flow velocities in the individual nozzles are known. This might be achieved with sophisticated instrumentation, but not likely without disturbing the aerosol flow itself, effectively invalidating the measurement attempt. So, when radial flow non-uniformity of the kind presented in this study exists, knowledge of the mass-average stage efficiency curve does not enable the size of particles captured on a stage to be determined. Indeed, it is false to state that the particles on the stage

are larger than the mass-average D_{50} value. And, it is typical for the user to assume incorrectly that the flow through each nozzle is the same in use as it was during the reported calibration.

If we then further allow the presence of non-uniformity of flow velocity to create an initially induced maldistribution of the mass concentration of the monodisperse calibrant aerosol, Equation (2) can be rewritten as:

$$F(d_{ae}) = \frac{\sum_{i=1}^{N} U_i m_i(d_{ae}) E_i(d_{ae}, U_i)}{\sum_{i=1}^{N} U_i m_i(d_{ae})} \quad [4]$$

for a given stage. Here, $m_i(d_{ae})$ is the mass concentration of particles of size d_{ae} at nozzle i of the array.

Equation (4) indicates that to assign a size to the particles captured by the given stage, we must determine the solution to Equation (5), which is difficult to solve analytically, since the values of $m_i(d_{ae})$ are not known *a priori*:

$$0.5 = \frac{\sum_{i=1}^{N} U_i m_i(d_{ae}) E_i(d_{ae}, U_i)}{\sum_{i=1}^{N} U_i m_i(d_{ae})} \quad [5]$$

In summary, the presence of non-uniformity of the radial flow velocity profile immediately before the entry to the nozzles of a given stage, as described in this article, makes it impossible to tell what size the particles are that have been classified by that stage, because the individual nozzle velocities are unknown *and* the point-wise mass concentration of particles may also not be known. When the inlet aerosol is polydisperse, the same equations pertain, but become even more intractable because the local point values of $m_i(d_{ae})$ are not known across the nozzle array.

It follows that the behavior we have observed with the uppermost two stages of the ACI, has to be treated as a highly detrimental factor for successful data interpretation of any cascade impactor stage affected by this process. Such an outcome causes a substantial disconnect, when considering how a polydisperse aerosol might behave as it approaches the nozzle plate, between the mass-average collection efficiency curve for that stage and the actual size of the collected particles. For this reason, multi-nozzle stage calibration curves, such as those shown in Figure 3 and commonly encountered in the literature associated with impactor performance verification (Mitchell et al. 1987; Vaughan 1989), are meaningful only if the radial flow velocity distribution across the nozzle array is the same in use as in the calibration.

It is important to note that impactor designs in which the initial size fractionating stage contains only a single nozzle aligned on axis with the incoming flow, as found, for example, with the Marple-Miller series of cascade impactors (Marple et al. 1995) and with the NGI (Marple et al. 2003a) are least vulnerable to flow maldistribution. Furthermore, since the particles arriving at the impactor inlet are in general larger than about 5-μm aerodynamic diameter, and therefore have significant inertia at this location, the probability of spatially dependent particle mass concentrations or size distributions occurring at the plenum immediately above the nozzle plate is greatly reduced, if not avoided altogether, if there is only a single inlet nozzle for the aerosol to penetrate. We acknowledge that these principles were likely not known at the time of the design of the modified stages "0" and "1" of the Mark-II ACI (the currently available design) was created.

Conclusions

We have demonstrated experimentally that the deposits collected under the uppermost stages "0" and "1" of an ACI operated at 28.3 L/min vary with the size of the particles presented to either stage, based on measurements employing monodisperse aerosols of differing mean size. Our finding is indicative of both non-uniformity of the flow velocity profile immediately upstream of either stage and very likely the presence of a size-dependent aerosol concentration maldistribution. The observed phenomenon can be understood by inertial size separation of the particles initiated by the existence of flow recirculation in the zone immediately before the entry plane to the nozzles of the size-fractionating stage. As a consequence, the true aerodynamic particle size distribution of an unknown input aerosol remains uncertain, even though the mass-average stage efficiency curve and associated D_{50} cut point size are known from published data generated by traditional calibration methods. We caution that this uncertainty will pertain, when the particles are coarser than about 5-μm aerodynamic diameter, to any impactor in which a non-uniform air flow velocity profile exists at the nozzle plate entry for the affected size-fractionating stages. Furthermore, standard methods of calibrating impactor stages have not taken into account the non-ideal flow velocity profiles of the actual, in-use situation. Indeed such methods mask the detailed size-fractionating behavior that obscures the particle aerodynamic size assessment of unknown aerosols. Finally, impactor designers must carefully assess the influence of the significant particle inertia that exists when choosing nozzle arrays for the size-fractionation of such coarse particles.

Nomenclature

A_i	area of nozzle "*i*"
d_{ae}	aerodynamic particle diameter
D_{50}	the aerodynamic size of particle captured with 50% efficiency
$E_i(d_{ae}, U_i)$	the fraction of particles of size d_{ae} passing through nozzle "*i*" at a velocity U_i captured on the impaction surface
$F(d_{ae})$	the fraction of particles of size d_{ae} captured on the impaction surface
U_i	average velocity of air at the exit of nozzle "*i*"

Acknowledgments

References

Andersen, A. (1958). A Sampler for Respiratory Health Assessment. *Am. Ind. Hyg. Assoc. J.* 27:160–165.

Berglund, R. N., and Liu, B. Y. H. (1973). Generation of Monodisperse Aerosol Standards. *Environ. Sci. Technol.* 7(2):147–153.

Blevins, R. D. (1984). *Theoretical Diffuser Performance.* Applied Fluid Dynamics Handbook, Van Nostrand Reinhold, NY, USA, pp. 144–161.

Byron, P. R., Cummings, R. H., Nichols, S. C., Poochikian, G., Smurthwaite, M. J., Stein, S. W., and Truman, K. G. (2004). Selection and Validation of Cascade Impactor Test Methods, in *Respiratory Drug Delivery—IX*, R. N. Dalby, P. R. Byron, J. Peart, J. D. Suman, and S. J. Farr, eds, Davis Healthcare International Publishing, River Grove, IL, USA, pp. 169–178.

Christopher, D., Curry, P., Doub, W., Furnkranz, K., Lavery, M., Lin, K., Lyapustina, S., Mitchell, J., Rogers, B., Strickland, H., Tougas, T., Tsong, Y., and Wyka, B. (2003). Considerations for the Development and Practice of Cascade Impaction Testing Including a Mass Balance Failure Investigation Tree. *J. Aerosol Med.* 16(3):235–247.

Dechraksa, J., Suwandecha, T., Maliwan, K., and Srichana, T. (2014). The Comparison of Fluid Dynamics Parameters in an Andersen Cascade Impactor Equipped with and Without a Preseparator. *AAPS Pharm Sci Tech.* 15(3):792–801.

Duan, H., Romay, F. J., Li, C., Naqwi, A., Deng, W., and Liu, B. Y. H. (2016). Generation of Monodisperse Aerosols by Combining Aerodynamic Flow-Focusing and Mechanical Perturbation. *Aerosol Sci. Technol.* 50(1):1–9.

Dunbar, C., and Mitchell, J. (2005). Analysis of Cascade Impactor Mass Distributions. *J. Aerosol Med.* 18(4):439–451.

European Pharmacopoeia (2016). *Section 2.9.18 Preparations for Inhalation, European Directorate for the Quality of Medicines (EDQM)*, Edition 8.8, Strassburg, France.

Fang, C. P., Marple, V. A., and Rubow, K. L. (1991). Influence of Cross-Flow on Particle Collection Characteristics of Multi-Nozzle Impactors. *J. Aerosol Sci.* 22:403–415.

Flynn, S. J., Tong, Z. B., Yang, R. Y., Kamiya, H., Yu, A. B., and Chan, H. K. (2015). Computational Fluid Dynamics (CFD) Investigation of the Gas-Solid Flow and Performance of the Andersen Cascade Impactor. *Powder Technology*, 285:128–137.

Govier, G. W., and Aziz, K. (1972). *The Flow of Complex Mixtures in Pipes.* Van Nostrand Reinhold, New York.

Marple, V. A. (1970). *A Fundamental Study of Inertial Impactors.* Ph.D. Thesis, University of Minnesota, Department of Mechanical Engineering, September 1970.

Marple, V. A., and Liu, B. Y. H. (1974). Characteristics of Laminar Jet Impactors. *Environ. Sci. Technol.* 8(7):648–654.

Marple, V. A., and Chien, C. M. (1980). Virtual Impactors: A Theoretical Study. *Environ. Sci. Technol.* 14(8):976–985.

Marple, V. A., Olson, B. A., and Miller, N. C. (1995). A Low-Loss Cascade Impactor with Stage Collection Cups: Calibration and Pharmaceutical Inhaler Applications. *Aerosol Sci. Technol.* 22(1):124–134.

Marple, V. A., Roberts, D. L., Romay, F. J., Miller, N. C., Truman, K. G., Van Oort, Olsson, B., Holroyd, M. J., Mitchell, J. P., and Hochrainer, D. (2003a) Next Generation pharmaceutical Impactor, Part I: Design. *J. Aerosol Med.* 16(3):283–299.

Marple, V. A., Olson, B. A., Santhanakrishnan, K., Mitchell, J. P., Murray, S. C., and Hudson-Curtis, B. L. (2003b). Next Generation Pharmaceutical Impactor—Part II: Archival Calibration. *J. Aerosol Med.* 16(3):301–324.

McFarland, A. R., Wedding, J. B., and Cermak, J. E. (1977). Wind Tunnel Evaluation of a Modified Andersen Impactor and an All Weather Sampler Inlet. *Atmos. Environ.* 11(6):535–539.

Mitchell, J.P., Costa, P.A., Waters, S. (1987). An Assessment of an Andersen Mark-II Cascade Impactor. *J. Aerosol Sci.* 19(2):213–221.

Mitchell, J., Nagel, M. (2003). Cascade Impactors for the Size Characterization of Aerosols from Medical Inhalers: Their Uses and Limitations. *J. Aerosol Med.* 16(3):341–377.

Mohammed, H., Roberts, D. L., Copley, M., Hammond, M., Nichols, S. C., and Mitchell, J. P. (2012). Effect of Sampling Volume on Dry Powder Inhaler (DPI)-Emitted Aerosol Aerodynamic Particle Size Distributions (APSDs) Measured by the Next Generation Pharmaceutical Impactor (NGI) and the Andersen Eight-Stage Cascade Impactor (ACI). *AAPS Pharm Sci Tech.* 13(3):875–882.

Pui, D. Y. H., Romay, F. J., and Liu, B. Y. H. (1987). Experimental Study of Particle Deposition in Bends of Circular Cross Section. *Aerosol Sci. Technol.* 7:301–315.

Roberts, D. L., and Mitchell, J.P. (2013). The Effect of Non-Ideal Impactor Stage Collection Efficiency Curves on the Interpretation of the Size of Inhaler-Generated Aerosols. *AAPS Pharm Sci Tech.* 14(2):497–510.

Roberts, D. L., and Mitchell, J.P. (2014). Deposit Maldistribution in the Andersen Non-Viable Mark-II Cascade Impactor (ACI): An Initial Investigation. *Drug Deliv Lungs* 25:154–158.

Roberts, D. L., Lavarreda, C., Milhomme, K., and Shelton, C. (2006). Managing Impactor Quality with Measurements of Flow Resistance and Effective Diameter. *Drug Deliv Lungs* 17:243–246.

Roberts, D. L. (2009). Theory of Multi-Nozzle Impactor Stages and the Interpretation of Stage Mensuration Data. *Aerosol Sci. Tech.*, 43:1119–1129.

Siegford, K. L., Marple, V. A., and Rubow, K. L. (1994). A Multiplet Reduction Impactor for the Vibrating Orifice Aerosol Generator. *J. Aerosol Sci.* 25:113–114.

Son, Y.-J., Mitchell, J. P., and McConville, J. T. (2011). *In vitro* Performance Testing for Pulmonary Drug Delivery, in *Controlled Pulmonary Drug Delivery*, H. D. C. Smyth, A. J. Hickey, eds., Springer, NY, USA, pp. 383–415.

United States Pharmacopeia. (2016). USP 39-NF 34, Chapter 601, Inhalation and Nasal Drug Products: Aerosols, Sprays and Powders – Performance Quality Tests. Rockville, MD, USA.

Versteeg, H. K., Zhao, P., Blatchford, C., Copley, M., Roberts, D. L., and Mitchell, J. P. (2015). A Computational Fluid Dynamics (CFD) Model of the Start-up Kinetics of the Andersen Cascade Impactor (ACI). *Drug Deliv Lungs* 26:18–21.

Vaughan, N. P. (1989). The Andersen Impactor: Calibration, Wall Losses, and Numerical Simulation. *J. Aerosol Sci.* 20 (1):67–90.

Zhou, Y., J. Sun, Y.-S. Cheng (2011). Comparison of Deposition in the USP and Physical Mouth-Throat Models with Solid and Liquid Particles. *J. Aero. Med. Pulmon. Drug Del.* 24:277–284.